ANS RPSD 2018 - 20th Topical Meeting of the Radiation Protection & Shielding Division of ANS
Santa Fe, NM, August 26 – 31, 2018, on CD-ROM, American Nuclear Society, LaGrange Park, IL (2018)

UPDATE OF THE NUCLEAR CRITICALITY SLIDE RULE CALCULATIONS: STUDIES WITH COMMON SHIELDING MATERIALS

T. M. Miller[1], C. Celik[1], C. Hopper[1], M. Duluc[2], D. Heinrichs[3], S. Kim[3], A. Brown[4], C. Wilson[4], and M. Troisne[5]

[1]*Oak Ridge National Laboratory, P.O. Box 2008, Oak Ridge, TN, 37831, USA millertm@ornl.gov*
[2]*Institut de Radioprotection et de Sûreté Nucléaire, B.P. 17, 92262 Fontenay-aux-Roses Cedex, France*
[3]*Lawrence Livermore National Laboratory, 7000 East Avenue, Livermore, CA, 94551, USA*
[4]*Atomic Weapons Establishment, Aldermaston, Reading, RG7 4PR, United Kingdom*
[5]*Millennium, 16 avenue du Québec – SILIC 628, 91945 Courtabœuf, France*

This paper presents preliminary results from the third phase of the current update to the nuclear criticality slide rule, in which MCNP, MAVRIC/Monaco, and COG have simulated the prompt neutron and photon dose from critical spheres of 4.95% enriched uranyl fluoride solution and 93.2% enriched uranium metal. New to this phase is the inclusion of various thicknesses of lead, steel, concrete, and water shielding. This phase also evaluated the effects of humidity on the unshielded configurations in the first phase, as well as the effects of changing the ground composition used in the first phase from concrete to dry soil. The small sample of results presented show that MCNP, MAVRIC/Monaco, and COG results are statistically the same or different by only a few percent. The impact of the shielding materials depends on their thickness, but doses decreased by nearly a factor of 100 are presented. In a few instances, buildup of gamma doses occurs due to neutron interactions in shielding materials.

I. INTRODUCTION

In January 1974, "A Slide Rule for Estimating Nuclear Criticality Information" was written by C. M. Hopper for the Oak Ridge Y-12 Plant as a tool for emergency response to nuclear criticality accidents.[1] In 1997, the Oak Ridge National Laboratory (ORNL) updated the report,[2,3] and in 2000, the Institut de Radioprotection et de Sûreté Nucléaire (IRSN) produced a similar report.[4] In 2016, ORNL, IRSN, Lawrence Livermore National Laboratory (LLNL), and the Atomic Weapons Establishment (AWE) began updating the nuclear criticality slide rule using modern radiation transport codes and nuclear data and introducing plutonium systems. This revision of the nuclear criticality slide rule will provide the same capabilities for continued updates to accident information during the evolution of emergency response to a criticality accident. These updates will include the same information as that included in previous slide rules: victim exposure information, potential exposures to emergency re-entry personnel, estimates of future radiation fields, and fission-yield estimates.

The slide rule permits the estimation of unknown parameters during a criticality accident using known parameters in the slide rule. For example, if the number of fission events is estimated, the slide rule can be used to estimate total prompt dose from the initial critical excursion or time dependent dose rate to personnel entering the facility at different times following the excursion. Alternatively, if dosimetry data is recovered from personnel exposed to the initial critical excursion, the number of fission events can be estimated based on the measured dose, position with respect to the criticality, and shielding.

This paper presents preliminary results from the third phase of the current update to the nuclear criticality slide rule. The first phase[5] repeated simulations from Broadhead and Hopper's reports[2,3] with modern radiation transport codes and nuclear data, and the second phase[6] introduced plutonium systems. In the phase discussed herein, MCNP[7], MAVRIC/Monaco[8], and COG[9] have simulated the prompt neutron and photon dose from critical spheres of 4.95% enriched uranyl fluoride solution and 93.2% enriched uranium metal which have undergone 10^{17} fission events with various thicknesses of lead, steel, concrete, and water shielding. This phase also evaluated effects of humidity on unshielded configurations in the first phase, as well as effects of changing the ground composition used in the analysis from concrete to dry soil.

The slide rule obviously cannot provide data for all possible criticality accidents. Users of the slide rule need to select the configuration available that best matches the actual scenario. This ongoing update intends to provide more configurations than previous slide rules, like plutonium systems, cylindrical systems, and critical systems with reflectors. This paper discusses updates and additions to the existing shielded configurations, which are useful for accidents where the critical system is shielded by a glove box, process water (maybe for cooling), a building with personnel outside, and so on.

II. CONFIGURATION DESCRIPTION

The critical uranium systems considered for the 1997 slide rule were as follows:

- Unreflected sphere of 4.95 wt% enriched uranyl fluoride
- Unreflected sphere of damp 5 wt% enriched UO_2
- Unreflected sphere of 93.2 wt% enriched uranyl nitrate
- Unreflected sphere of 93.2 wt% enriched uranium metal
- Unreflected sphere of damp 93.2 wt% enriched U_3O_8

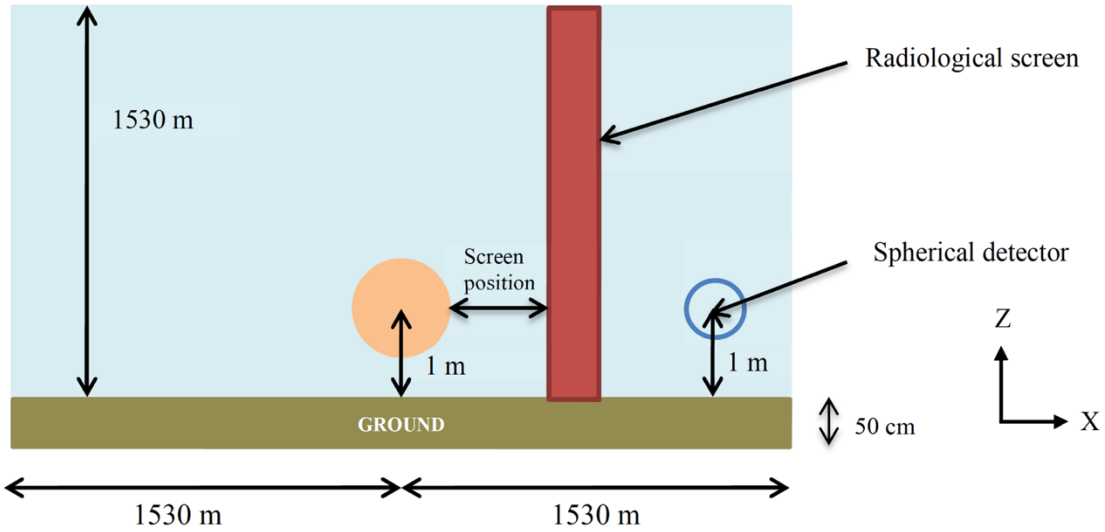

Fig. 1a. Shielded geometry configuration, XZ view.

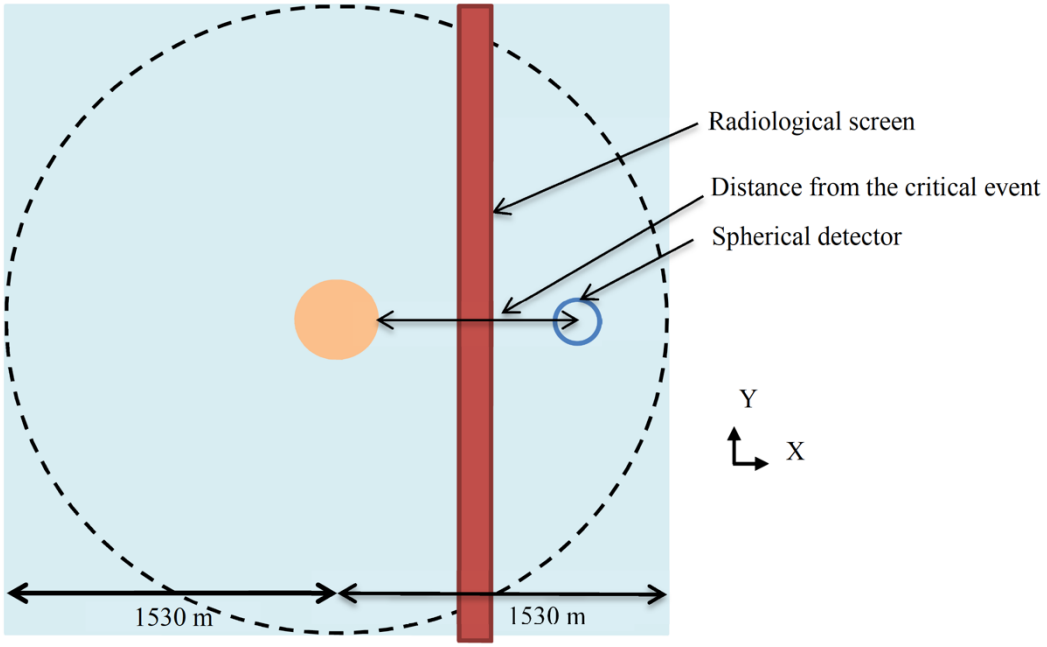

Fig. 1b. Shielded geometry configuration, XY view.

While Duluc's "Update of the Nuclear Criticality Slide Rule for the Emergency Response to a Nuclear Criticality Accident"[5] repeated all simulations performed by Broadhead and Hopper with modern radiation transport codes and nuclear data, this work is focused on the first and fourth configurations listed above: low enriched uranyl fluoride and highly enriched uranium metal. This covers both a large range of enrichment and a large range of hydrogen-to-uranium-235 atom ratio (410 to 0).

II.A. New Unshielded Configurations

The first two changes to the configurations in Duluc's update to the slide rule do not involve any shielding materials. Rather, these are changes to ground and air compositions. In Duluc's update, the ground is regulatory concrete[8] containing 1.0 wt% H. This work analyzes dry soil with no H, referred to as *Earth, US Average*, in McConn's "Compendium of Material Composition Data for Radiation Transport Modeling."[10] The air model in Duluc's update was dry air. In this study, a range of humid air will be considered: relative humidity of 10% and 100%

(0.016 and 0.163 wt% H). The resulting number densities are provided in Table I.

TABLE I. Humid air number densities (atom/b*cm).

Isotope	10% Humidity	100% Humidity
^{14}N	3.9214E-05	3.8397E-05
^{16}O	1.0798E-05	1.1094E-05
^{1}H	1.1559E-07	1.1559E-06

II.B. Shielded Configurations

The new shielded geometry configuration used in this work can be seen in Figure 1. There are two notable features of this geometry. First, the addition of the shield (radiological screen in Figure 1) dramatically changed the problem symmetry, which has an effect on run times for Monte Carlo simulations since the dose tallies will not be able to exploit any problem symmetry. Second, the shield is always halfway between the fissile material and tally location, as opposed to a fixed shield location, so a simulation is required for each tally location. Table II provides the shield or screen position shown in Figure 1a and the detector location or distance from the critical event shown in Figure 1b. Figure 1 indicates that the detector has a spherical shape, but this is simply a sphere of air. For detectors located 100 m or less from the critical event, the sphere has a radius of 20 cm. Beyond 100 m, the spherical detector has a radius of 40 cm. Four different shielding materials were considered: stainless steel 304, water, lead, and regulatory concrete. The compositions of the stainless steel, water, and lead were taken from McConn's compendium,[10] and these three materials were simulated with thicknesses of 1, 5, 10, and 20 cm. The regulatory concrete was simulated with thicknesses of 20 and 40 cm.

III. COMPUTATIONAL METHODOLOGY

This section describes the different codes and computational methods used by the laboratories contributing to this work. All groups involved used the same response functions to convert the simulated neutron and photon fluxes to doses; these are the flux-to-dose conversion factors published in the ANSI/HPS 13.3-2013 standard on criticality accident dosimetry.[11]

III.A. MCNP

MCNP6.1 was used with the continuous-energy ENDF/B-VII.1 cross section library provided with the code. An F4 tally (i.e., track length estimate of cell flux) in the spherical detector cell was used to calculate the neutron and photon fluxes, which were converted to doses with the flux-to-dose conversion factors mentioned above. For prompt doses, total nu-bar was used. Weight windows in space and energy generated by the ADVANTG[12] code were used.

For prompt doses considered in this paper, a two-step method was used. The first step is a KCODE calculation to determine the distribution of fission neutron production inside the uranium spheres. The fission reaction rate was tallied in 20 spherical mesh cells (SMESH), having the same volume. Due to the proximity of the ground below the critical system and the adjacent shielding materials, the spatial distribution of fission events in each sphere is not completely symmetric. The 1-D spherical mesh tally does not capture this asymmetry in the fission distribution. The second step used the results of the first step to describe a fixed source (SDEF) of fission neutrons. A Watt spectrum was used for the energy distribution. The prompt gamma and neutron doses were determined in the same calculation, the gammas being produced by the neutron interactions inside the uranium sphere. Indeed, in the second step, the fission neutron production was turned off (treated as absorption), but all gammas, including fission gammas, are produced (NONU = 0).

III.B. SCALE

SCALE 6.2.2 was used with the ENDF/B-VII.1 cross section data. The libraries used with KENO-VI and MAVRIC/Monaco both used a continuous-energy representation of the cross sections. The CAAS analysis capability, coupling KENO and MAVRIC/Monaco, was used for this analysis, which is almost identical to the two-step methodology used for the MCNP analysis.

First, KENO was run with a 3-D cartesian mesh tally of the fission neutron production which captured any asymmetry due to the ground being 1 m below the center of each fissile sphere and the adjacent shielding material. Then MAVRIC/Monaco used the KENO-VI tally as a fixed source, generated variance reduction parameters (weight windows and a consistent biased source), and simulated the prompt doses. Region tallies were used in the model, along with the ANSI/HPS flux-to-dose conversion factors, to calculate doses in the spherical detectors at the desired distances. For the prompt dose calculations, total nu-bar was used as in the MCNP calculations, and fission

Table II. Detector locations and shield positions.

Detector Location (m)	Shield Position(m)	Detector Location (m)	Shield Position(m)	Detector Location (m)	Shield Position(m)
1	0.5	50	25	700	350
2	1	100	50	1,000	500
5	2.5	200	100	1,200	600
10	5	300	150		
20	10	500	250		

neutron production was turned off while fission gamma production was turned on (fissionMult=0, secondaryMult=2).

III.C. COG

COG 11.2 was used with a cross section library based on the ENDF/B-VII.1 data. COG is a general purpose, multiparticle, high-fidelity Monte Carlo code developed by LLNL. It provides accurate simulation results for complex 3-D shielding, criticality safety, and activation problems. Point-wise continuous cross sections are used in COG, and biasing options are available for speeding up solutions for deep penetration problems.

A direct one-step criticality/detector calculation method was applied for all prompt neutron and photon dose calculations. All neutron and gamma particles are tracked from birth due to fission within the spherical fissile volume to absorption in or leakage from the system in one single, massively parallel, COG supercomputer run, with no variance reduction biasing applied. Both boundary crossing and point detector options were activated to score the dose calculations. The point detector option was used for the detector locations at great distances from the fissile sphere.

IV. SAMPLE RESULTS

The following subsections provide a small sample of preliminary results available at this writing. Note some individual results may be missing in the figures below, which is due to unfinished simulations at the time of writing. As a reminder, the results below are all normalized to 10^{17} fission events in each sphere. All the Monte Carlo results and ratios plotted include 2-sigma error bars, and all data series in the plots are labeled *N* for neutron and *P* for photon.

IV.A. New Unshielded Configurations

The ground composition and air humidity of the original slide rule configurations in Duluc's update to the slide rule[5] for uranyl fluoride and uranium metal were perturbed in this study. MCNP dose results for the humid air perturbations are presented in Figure 2, where the uranyl fluoride results are labeled C1 for case 1, and the uranium metal results are labeled C4 for case 4. The perturbations added humidity to the dry air in the original configuration. The air was modeled with 10% and 100% relative humidity for standard atmospheric temperature and pressure at sea level. For all detector locations, the neutron dose for the uranium metal sphere was greater than the neutron dose for the uranyl fluoride sphere because the neutrons leaving the metal sphere had a harder spectrum (were less moderated). For the photon dose, the opposite trend was true out to 300 m, as the uranyl fluoride dose was greater than uranium metal dose due to H capture in the solution. Beyond 300 m, the photon dose was approximately the same, regardless of the fissile material. The magnitude of the relative humidity had little effect on the dose for most cases.

The MCNP simulated results are compared to SCALE simulations in Figure 3. However, the simulation of the uranium metal sphere surrounded by air with 100% relative humidity was not complete at this stage. The SCALE and MCNP simulations are either statistically equivalent, or they differ by less than 5%. Figure 4 compares the MCNP and COG simulated results. Most of the COG and MCNP simulations are either statistically equivalent, or they differ by less than 5%. A few of the COG results at 700 m and beyond are not within 5% of the MCNP results, but the COG simulations did not use much variance reduction and might have benefitted from additional run time. The comparisons in Figures 2 and 3 are presented via ratios of the simulated results.

IV.B. Shielded Configurations

Four different shielding materials—stainless steel 304, water, lead, and concrete—were placed halfway between the uranium metal and uranyl fluoride critical spheres, and each detector was placed in the same location as in the original configuration. For the stainless steel 304, water, and lead shielding materials 1, 5, 10, and 20 cm of each material was evaluated.

The configuration in Figure 1 was modeled with two regulatory concrete shield thicknesses, 20 and 40 cm. The results of the doses simulated by MCNP are presented in Figure 5. For both the uranyl fluoride and uranium metal spheres with 20 cm of concrete shielding, initially the neutron dose was greater than the photon dose. At large distances, this trend was reversed. The photon dose became greater than the neutron dose due to the neutrons slowing down and producing capture gammas in air. This transition occurred at around 500 m. With 40 cm of concrete shielding, the photon dose was about the same (uranium metal) or greater (uranyl fluoride) than the neutron dose at small distances. As distance increased with the 40 cm shield, the photon dose increased as compared to the neutron dose, as was observed with the 20 cm concrete shield.

The MCNP simulated results with the concrete shields are compared to SCALE simulations in Figure 6. The SCALE and MCNP simulations are either statistically equivalent, or they differ by less than 10%. Figure 7 compares the MCNP and COG simulated results. Most of the COG and MCNP simulations are either statistically equivalent, or they differ by less than 10%. A few of the COG results at 500 m and beyond have uncertainties greater than 10% and would benefit from additional run time. The comparisons in Figures 6 and 7 are presented via ratios of the simulated results.

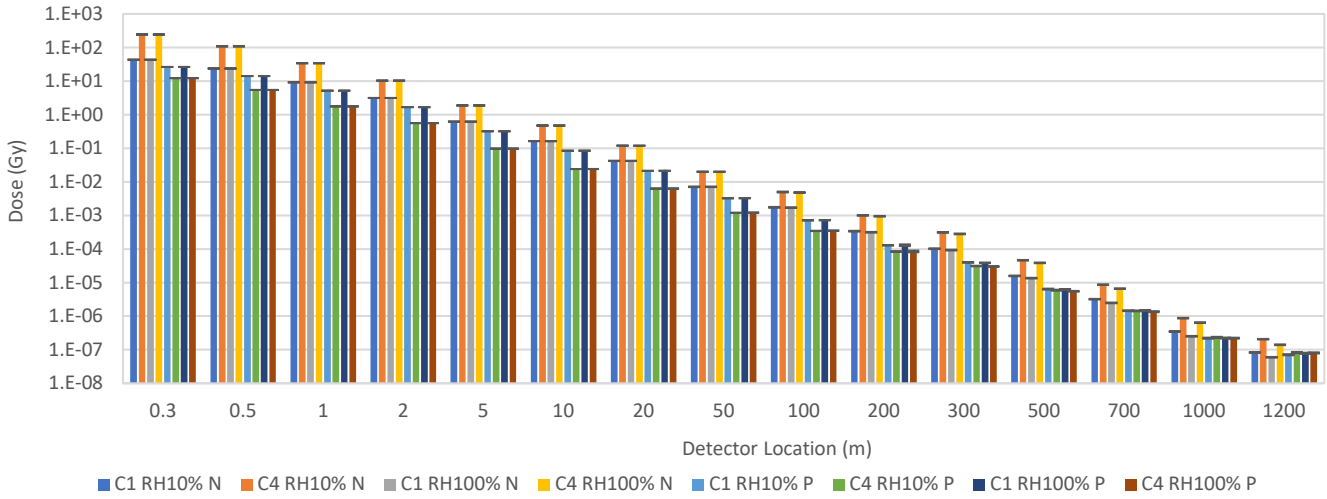

Fig. 2. MCNP simulated doses from critical uranium spheres surrounded by humid air.

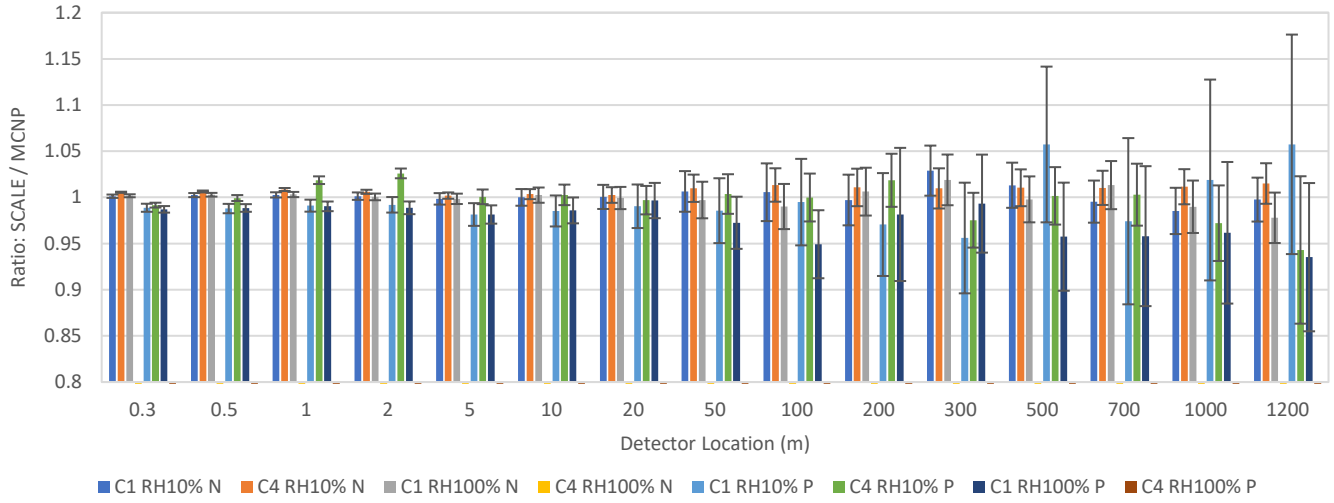

Fig. 3. SCALE-to-MCNP ratio of doses from critical uranium spheres surrounded by humid air.

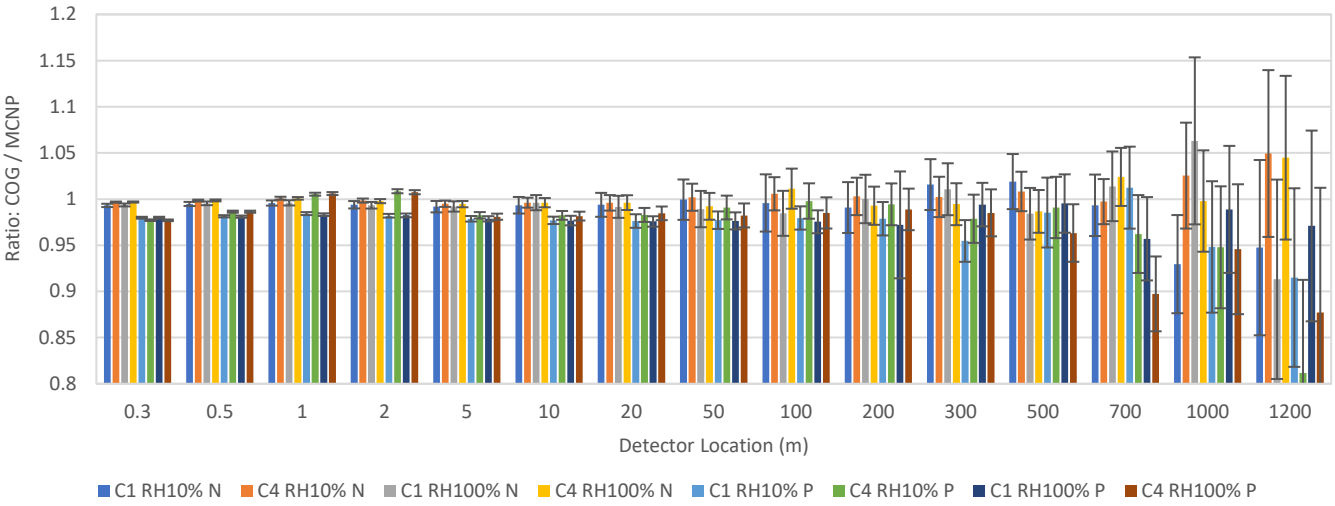

Fig. 4. COG-to-MCNP ratio of doses from critical uranium spheres surrounded by humid air.

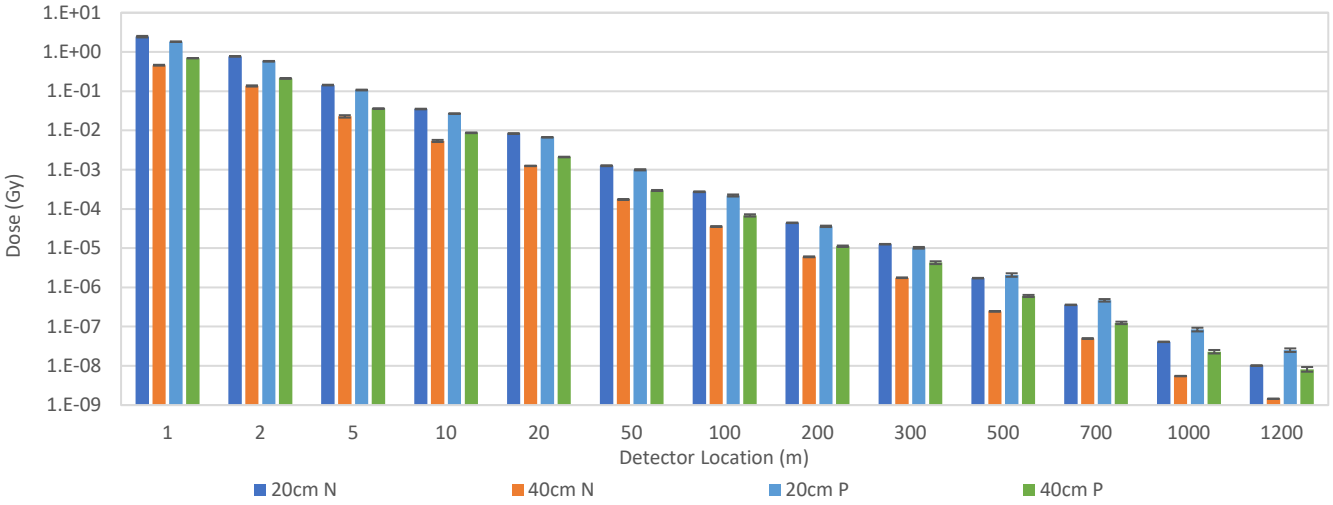

Fig. 5a. MCNP simulated doses from a critical U(4.95wt%)O_2F_2 sphere shielded by concrete.

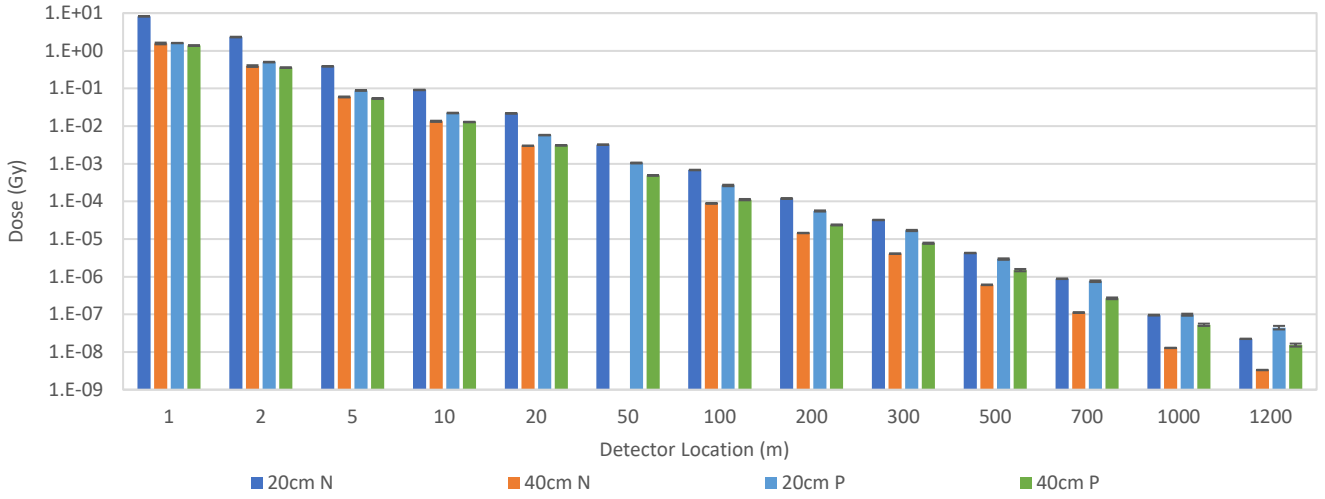

Fig. 5b. MCNP simulated doses from a critical U(93.2wt%) metal sphere shielded by concrete.

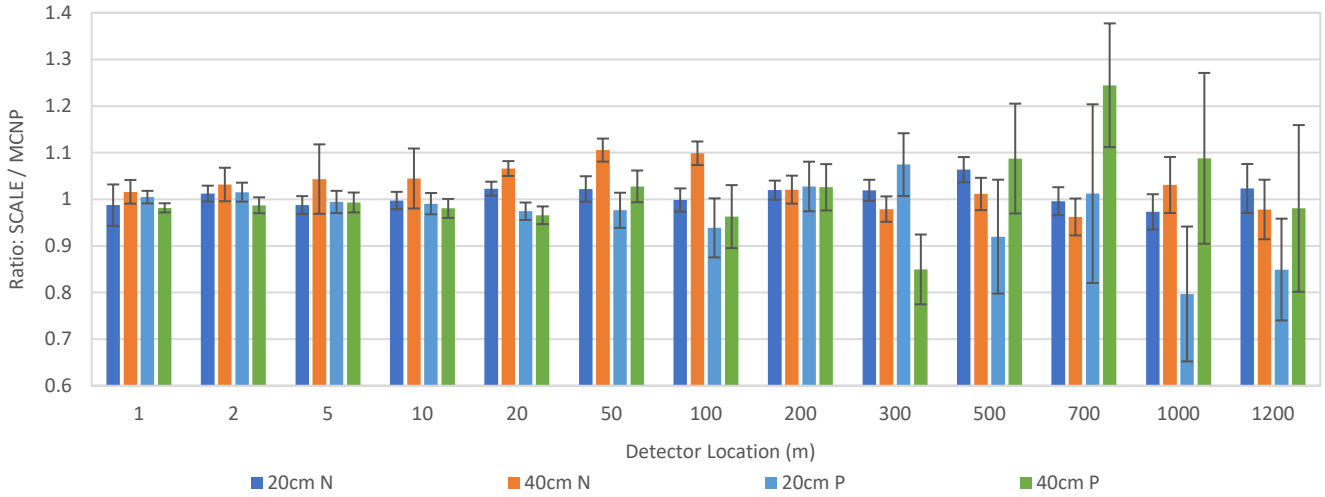

Fig. 6a. SCALE-to-MCNP ratio of doses from critical U(4.95wt%)O_2F_2 sphere shielded by concrete.

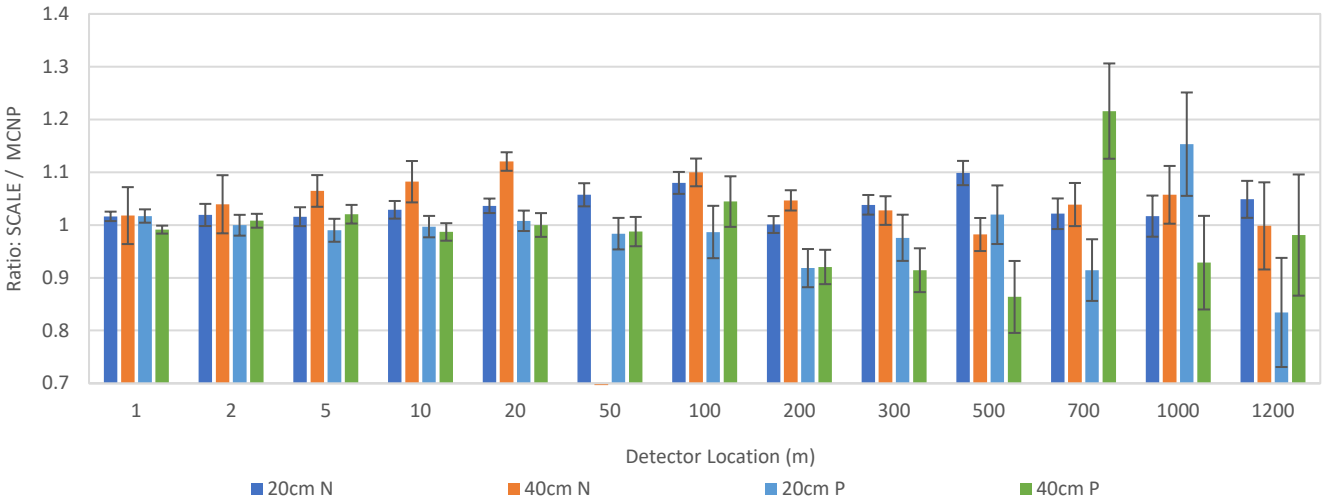

Fig. 6b. SCALE-to-MCNP ratio of doses from critical U(93.2wt%) metal sphere shielded by concrete.

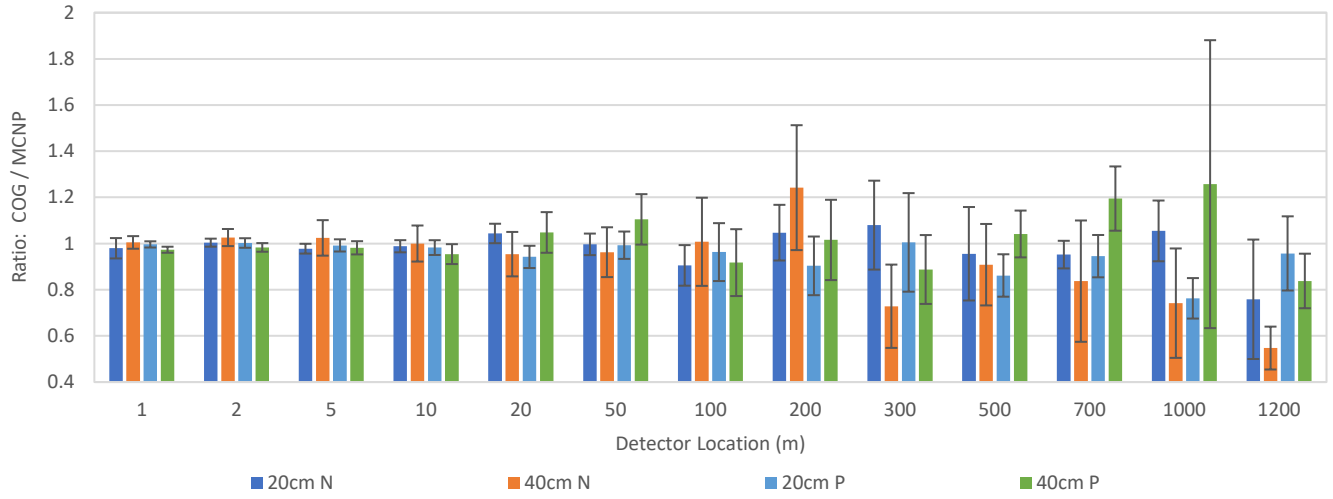

Fig. 7a. COG-to-MCNP ratio of doses from critical U(4.95wt%)O_2F_2 sphere shielded by concrete.

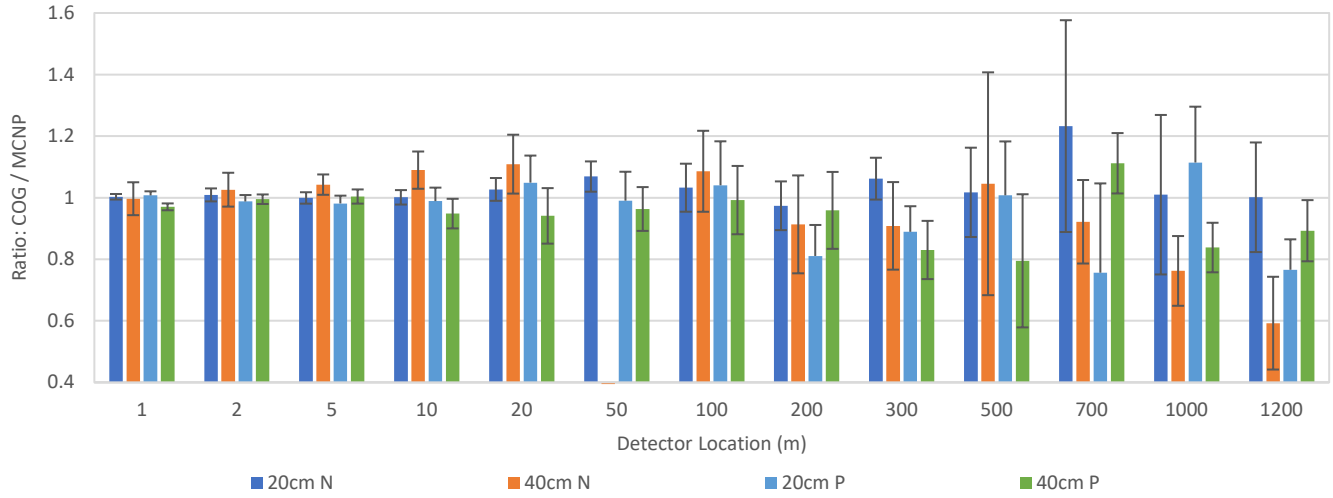

Fig. 7b. COG-to-MCNP ratio of doses from critical U(93.2wt%) metal sphere shielded by concrete.

V. CONCLUSIONS

The sample results presented in section IV are representative of all results completed at the time of writing. The agreement between MCNP, MAVRIC/Monaco, and COG is fairly good, with only small, statistically significant differences observed. A few simulations for shielded detectors at large distances from the critical spheres still need additional run time to improve the Monte Carlo statistics.

This section will make a few conclusions by comparing the new simulation results in section IV to the original systems discussed in reference 5. The original system is always the critical sphere surrounded by dry air, above regulatory concrete, and includes no shielding. As in the previous section, the error bars in the plots below represent 2-sigma uncertainty, the data series labeled *N* are neutron results, and those labeled *P* are photon results.

V.A. New Unshielded Configurations

Figure 8 shows how the humidity perturbation affects the simulated doses from the original configuration with dry air. The data in Figure 8 illustrate the ratio of the perturbed and original MCNP simulations. Out to 100 m, the humidity has very little effect on the doses. Beyond this point, the 100% relative humidity has the greatest effect, decreasing the neutron dose as much as 35%.

Figure 9 shows how the dry soil affects the simulated doses as compared to regulatory concrete. Changing the ground composition has a relatively small effect on the photon dose from the uranyl fluoride sphere. For the uranium metal sphere, the soil causes the photon dose to initially decrease as much as 40% and then increase back to a value similar to the original simulation. The soil causes the neutron dose to increase for both spheres, with a maximum increase of 70%.

V.B. Shielded Configurations

The impact each shielding material has on the original configurations is presented in Figures 10–13. This comparison is presented via the ratio of the perturbed simulations to the original simulations. Most of these comparisons are presented using the MCNP simulation results. In a few instances, the MCNP results were not available at the time of writing, so the SCALE results are used instead.

The impact of the water shield is presented in Figure 10 using SCALE simulation results. For the uranyl fluoride sphere (Figure 10a) the neutron and photon doses all decreased, and the decrease was only slightly dependent on the distance from the spheres. As expected, the dose was reduced more for thicker water shields. The largest neutron dose reduction was about 96% of the original and 50% for the photons. For the uranium metal sphere (Figure 10b), the effect on the neutron dose was very similar to the uranyl fluoride sphere. The largest decrease in neutron dose was about 97%. The photon dose initially increased almost by a factor of 2 due to the production of photons in the water shield, but at large distances, the photon dose reduction was very similar to the uranyl fluoride sphere, about 50%. For the water shield, the photon dose tended to be as large or larger than the neutron dose.

The impact of the stainless steel 304 shield is presented in Figure 11 using SCALE and MCNP simulation results. For the uranyl fluoride sphere (Figure 11a), the impact of the stainless steel 304 shield was very similar the water shield: the shield decreased the dose, and the thicker the shield, the greater the decrease. However, the neutron dose tended to be larger than the photon dose with the stainless-steel shield. The largest decreases for the neutron and photon doses were 87% and 97%, respectively. The neutron dose was decreased for the uranium metal sphere (Figure 11b) with the stainless-steel shield, and the photon dose increased slightly (at most 14%) out to about 200 m, and then it decreased. The largest decrease for both the neutron and photon doses was about 87%.

The impact of the lead shield is presented in Figure 12 using MCNP simulation results. The effect of the lead shield for the uranyl fluoride (Figure 12a) and uranium metal (Figure 12b) spheres was largely the same. The neutron and photon doses were always decreased by the lead shield, and the neutron doses were always larger than the photon doses. For the uranyl fluoride sphere, the largest decrease for the neutron and photon doses was 69% and 98%, respectively. For the uranium metal sphere, the decreases were 72% and 86%.

The impact of the regulatory concrete shield is presented in Figure 13 using MCNP simulation results. For the uranyl fluoride sphere (Figure 13a), the concrete shield always decreased the dose. This decrease leveled out at around 200 m for neutrons. At this point, the photon dose increased slightly. In all instances, the photon dose was larger than the neutron dose. The largest decreases for the neutron and photon doses were 98% and 91%, respectively. For the uranium metal sphere (Figure 13b) the neutron and photon doses were always decreased compared to the unshielded configuration. Additionally, the neutron dose and photon dose for the 40 cm thick concrete shield decreased out to about 300 m and then leveled out. However, the photon dose for the 20 cm thick shield built up out to about 10 m, and then it began to decrease. Like the uranyl nitrate sphere, the photon doses for the uranium metal sphere were always greater than the neutron doses. The largest decreases for the neutron and photon doses were 98% and 82%, respectively.

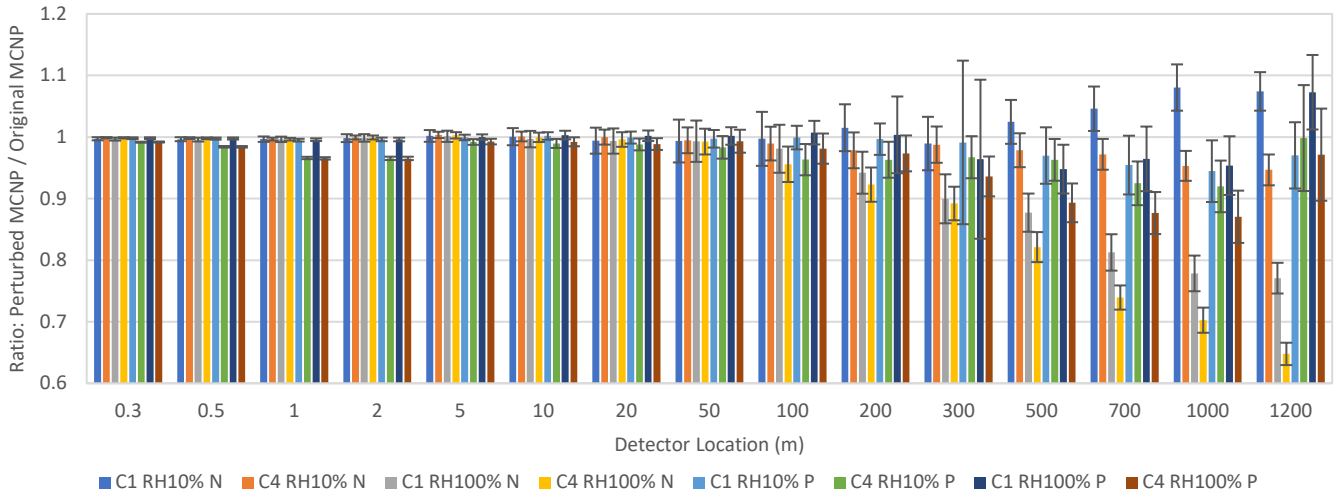

Fig. 8. Ratio of perturbed MCNP to original MCNP doses from critical uranium spheres surrounded by humid air.

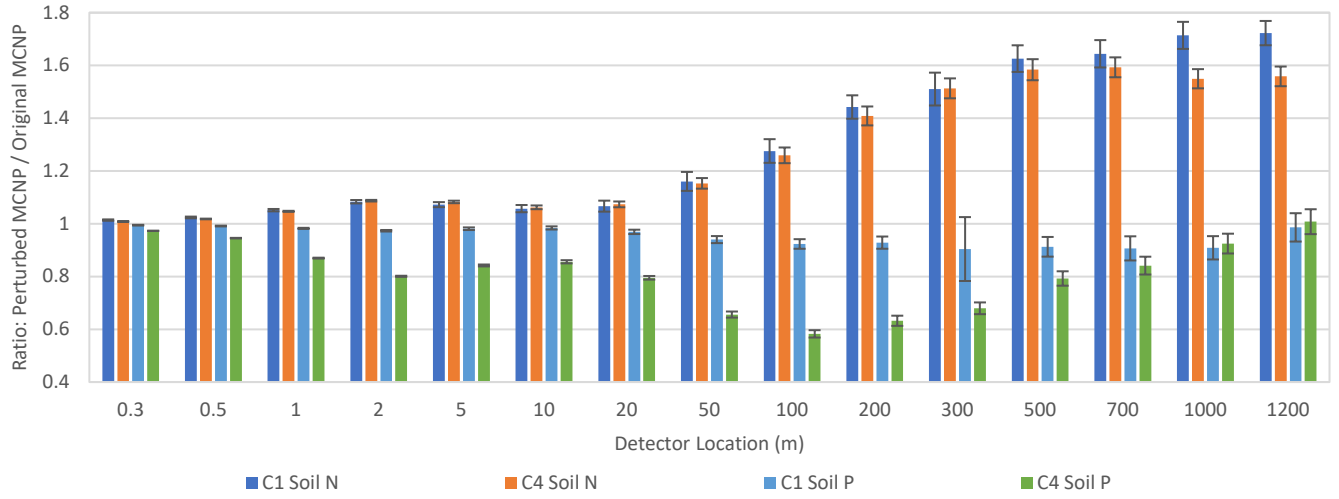

Fig. 9. Ratio of perturbed MCNP to original MCNP doses from critical uranium spheres above dry soil.

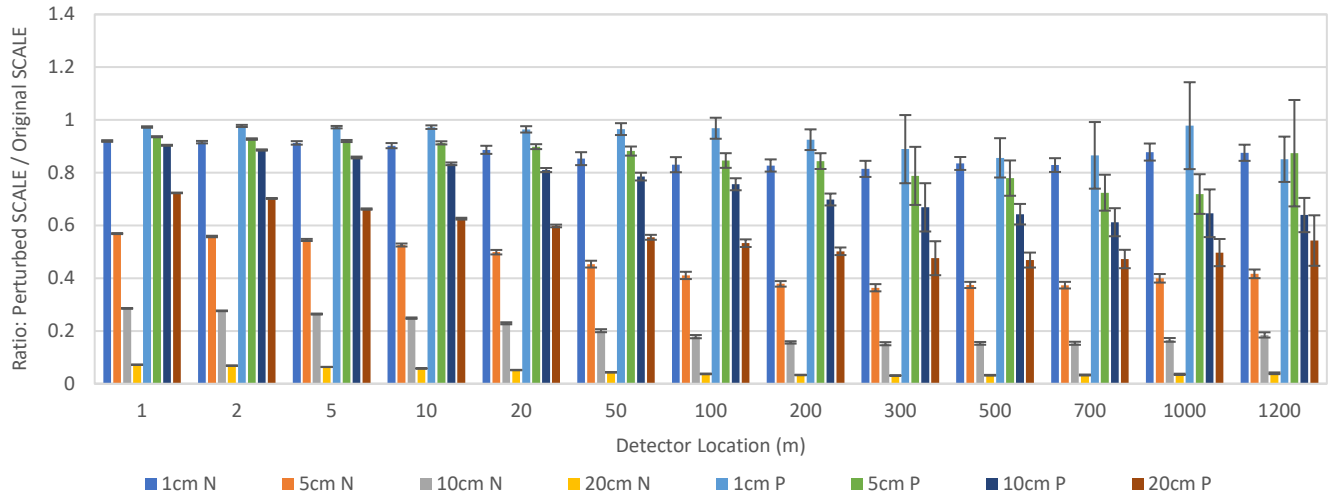

Fig. 10a. Ratio of perturbed SCALE to original SCALE doses from critical U(4.95wt%)O_2F_2 sphere shielded by water.

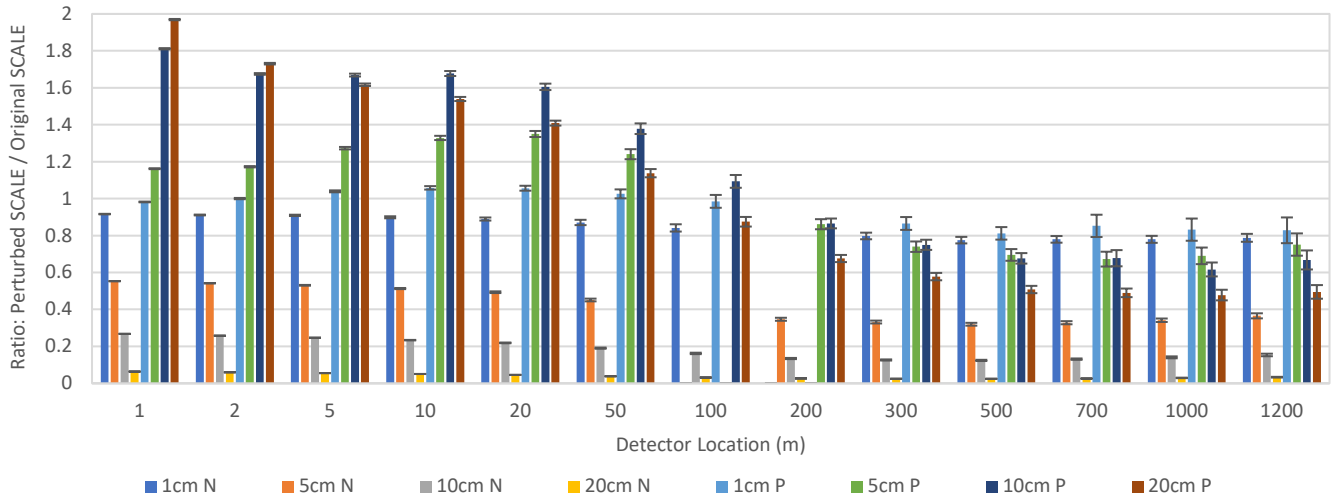

Fig. 10b. Ratio of perturbed SCALE to original SCALE doses from critical U(93.2wt%) metal sphere shielded by water.

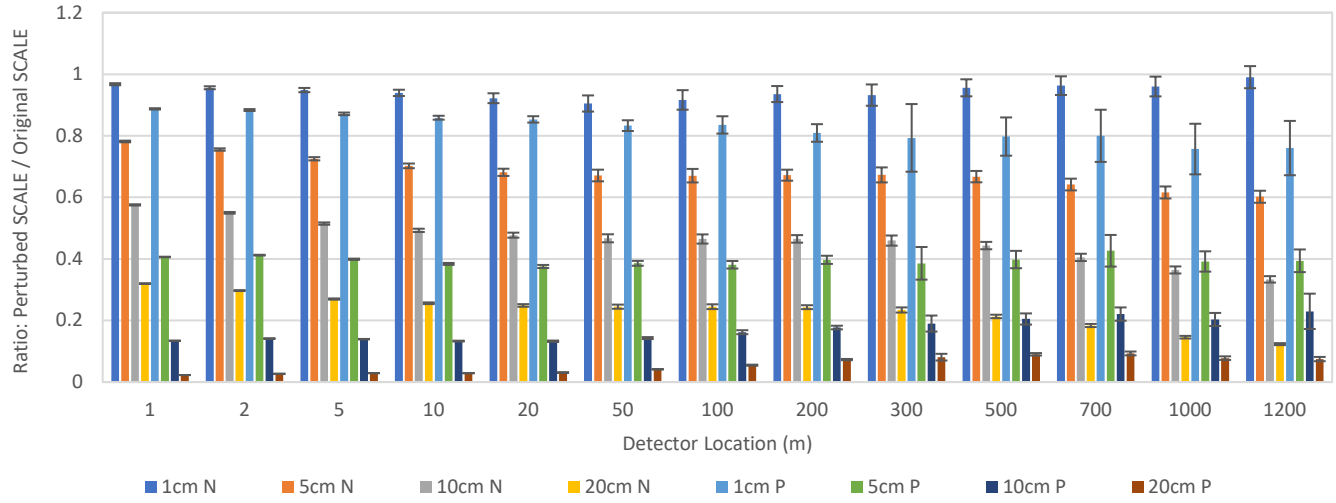

Fig. 11a. Ratio of perturbed SCALE to original SCALE doses from critical U(4.95wt%)O_2F_2 sphere shielded by SS304.

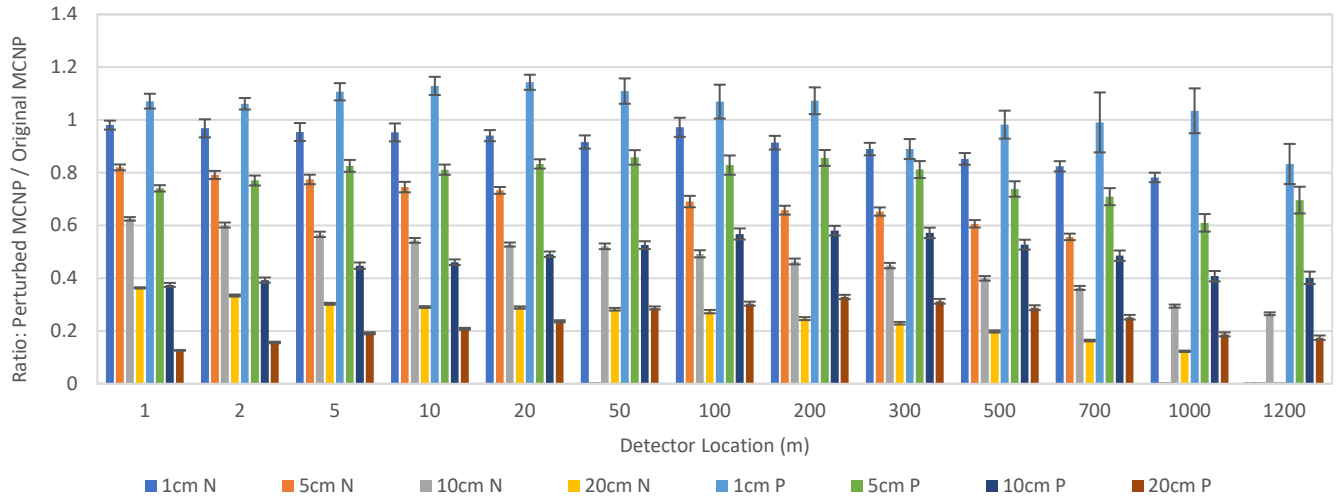

Fig. 11b. Ratio of perturbed MCNP to original MCNP doses from critical U(93.2wt%) metal sphere shielded by SS304.

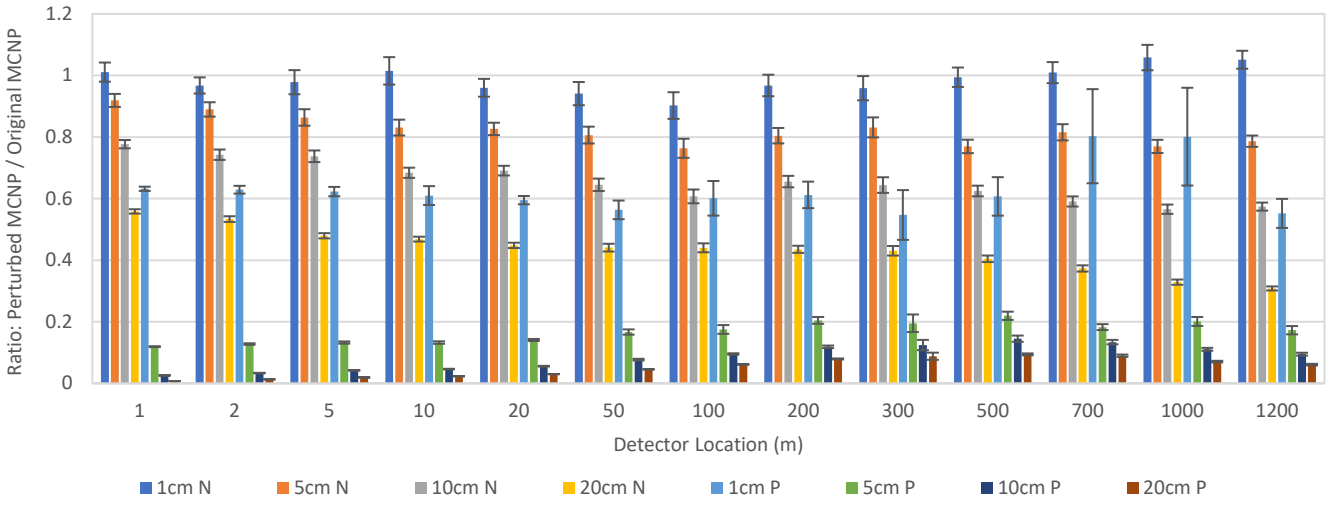

Fig. 12a. Ratio of perturbed MCNP to original MCNP doses from critical U(4.95wt%)O_2F_2 sphere shielded by lead.

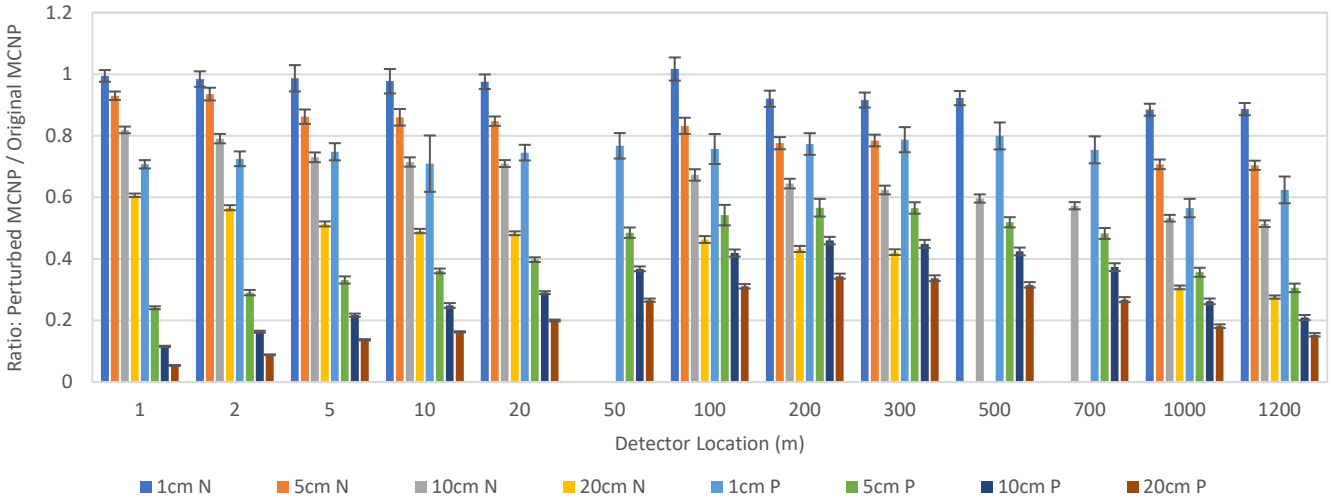

Fig. 12b. Ratio of perturbed MCNP to original MCNP doses from critical U(93.2wt%) metal sphere shielded by lead.

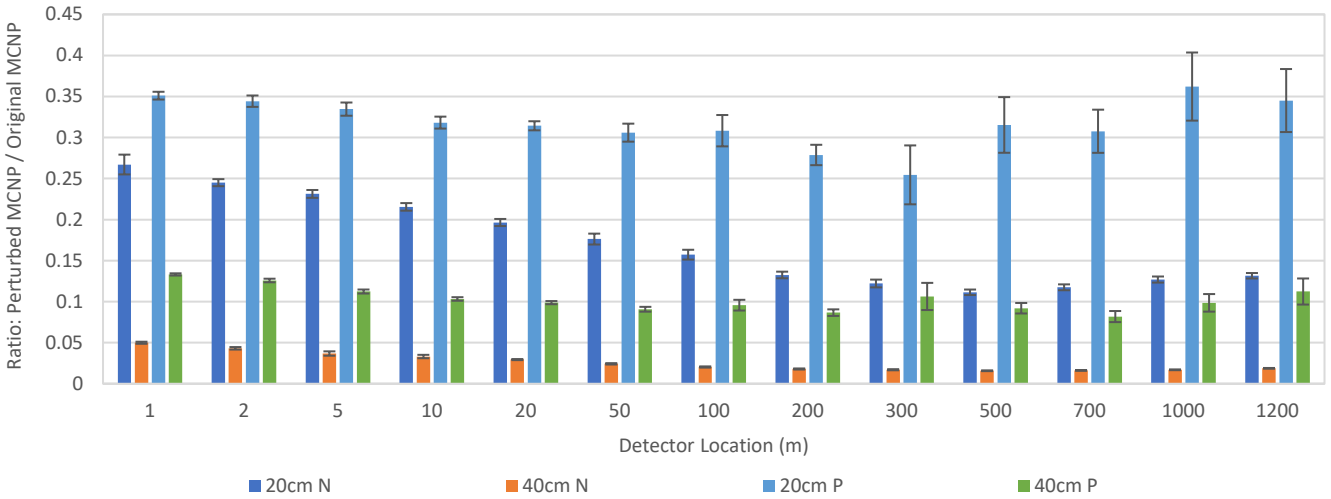

Fig. 13a. Ratio of perturbed MCNP to original MCNP doses from critical U(4.95wt%)O_2F_2 sphere shielded by concrete.

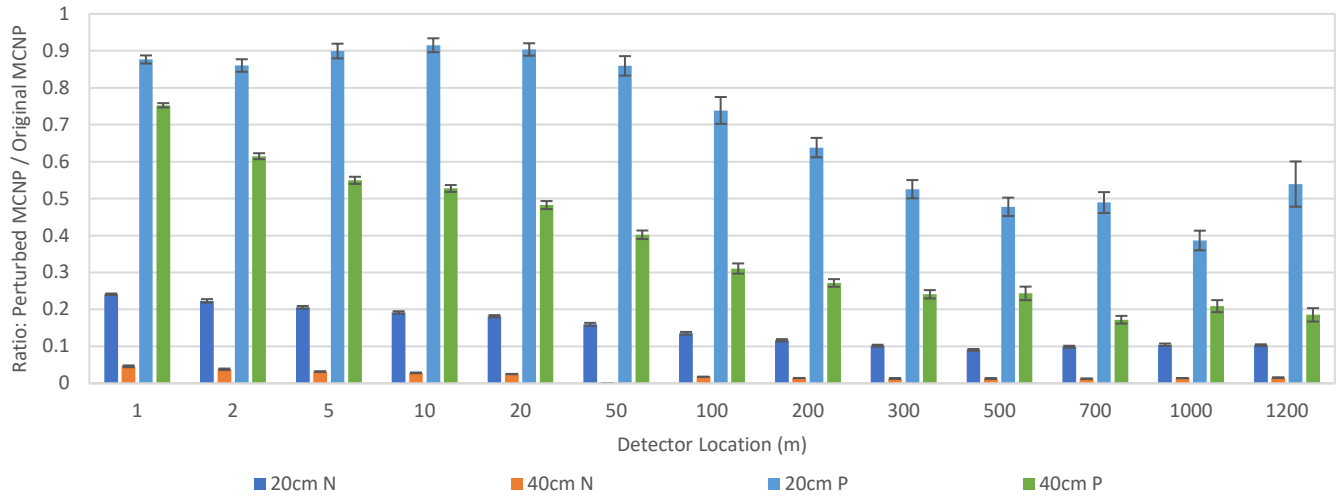

Fig. 13b. Ratio of perturbed MCNP to original MCNP doses from critical U(93.2wt%) metal sphere shielded by concrete.

ACKNOWLEDGMENTS

The contribution to this work by ORNL was funded by the United States Department of Energy Nuclear Criticality Safety Program (NCSP).

This work was performed under the auspices of the US Department of Energy by Lawrence Livermore National Laboratory under Contract DE-AC52-07NA27344 and was funded by the US Department of Energy Nuclear Criticality Safety Program.

REFERENCES

1. C. M. HOPPER, *Slide Rule for Estimating Nuclear Criticality Information*, Y-DD-145, Union Carbide Corporation, Nuclear Division, Oak Ridge National Laboratory (1974).
2. B. L. BROADHEAD et al., *An Updated Nuclear Criticality Slide Rule: Technical Basis*, NUREG/CR-6504 Vol. 1, ORNL/TM-13322/V1, Oak Ridge National Laboratory (1997).
3. C. M. HOPPER and B. L. BROADHEAD, *An Updated Nuclear Criticality Slide Rule: Functional Slide Rule*, NUREG/CR-6504, Vol. 2, ORNL/TM-13322/V2, Oak Ridge National Laboratory (1998).
4. *Fiches Accident-Type*, IRSN internal report (2000).
5. M. DULUC et al., "Update of the Nuclear Criticality Slide Rule for the Emergency Response to a Nuclear Criticality Accident," *EPJ Web of Conferences*, **153**, 05015 (2017).
6. M. DULUC et al., "Introduction of Plutonium Systems to the Nuclear Criticality Slide Rule," *Proceeding of the 2017 Nuclear Criticality Safety Division Topical*, Carlsbad, New Mexico, USA, September 10–15, 2017, American Nuclear Society (2017).
7. MCNP6 Development Team, *MCNP6 User's Manual, Version 1.0*, LA-CP-13-00634, Rev. 0, Los Alamos National Laboratory (May 2013).
8. B. T. REARDEN and M. A. JESSEE, *SCALE Code System*, ORNL/TM-2005/39, Version 6.2.2, Oak Ridge National Laboratory (February 2017).
9. R. M. BUCK and E. M. LENT, *COG11.1 Manual Supplement 2.15*, LLNL-SM-635621, Lawrence Livermore National Laboratory (April 2013).
10. R. J. MCCONN, et al., *Compendium of Material Composition Data for Radiation Transport Modeling*, PNNL-15870 Rev. 1, Pacific Northwest National Laboratory (2011).
11. *Dosimetry for Criticality Accidents*, ANSI-HPS 13.3-2013, American National Standards Institute, Inc. (2013).
12. S. W. MOSHER, et al., *ADVANTG—An Automated Variance Reduction Parameter Generator*, ORNL/TM-2013/416 Rev. 1, Oak Ridge National Laboratory (2015).